ADVANCED FUNCTIONAL MATERIALS
www.afm-journal.de

Plasmonic-Assisted Graphene Oxide Films with Enhanced Photothermal Actuation for Soft Robots

*Yuanyuan Yang, Yanting Liu, and Yajing Shen**

Carbon-based materials are widely used as light-driven soft actuators relying on their thermal desorption or expansion. However, applying a passive layer in such film construction greatly limits the actuating efficiency, e.g., bending amplitude and speed. In this work, a dual active layer strengthened bilayer composite film made of graphene oxide (GO)–polydopamine (PDA)–gold nanoparticles (Au NPs)/polydimethylsiloxane (PDMS) is developed. In this film, the conventional passive layer is replaced by another AuNPs-enhanced thermal responsive layer. When applying NIR light exposure, the whole film deforms controllably resulting from the water loss in the GO–PDA–Au NPs layer and thermal expansion in the PDMS layer. Benefiting from the dual active bilayer mechanism, the thin film's actuating efficiency is dramatically improved compared with that of conventional methods. Specifically, the bending amplitude is enhanced up to 173%, and the actuating speed is improved to 3.5-fold. The soft actuator can act as an artificial arm with high actuating strength and can be used as a wireless gripper. Moreover, the film can be designed as soft robots with various locomotion modes including linear, rolling, and steering motions. The developed composite film offers new opportunities for biomimetic soft robotics as well as future applications.

1. Introduction

Recently, diverse small soft robotics have been developed by mimicking living species,[1,2] wherein soft actuator is the key component to realize all kinds of motions. Up to now, several materials have demonstrated the ability of soft actuators based on different driving mechanisms, including but not limited to electric, magnetic, thermal, chemical, and optical fields.[3–10] Among all these methods, optical driving exhibits high adjustability because the material can be selectively triggered by light spot remotely without electromagnetic disturbance.[11–16] Owning to the high photothermal efficiency and mechanical strength, carbon-based materials have received increasing interest and been considered as promising candidates for light-driven actuators.[17–25] For instance, the graphene oxide (GO)–polydopamine (PDA)/reduced graphene oxide (rGO)[26] and carbon nanotube (CNT)/polydimethylsiloxane (PDMS)[27] composite films are capable of reversible light-actuated bending. Carbon-based bilayer actuators have proven their value in the fields of artificial muscles and biomimetic robotics.

In the existing approaches, the carbon material-based films are usually designed with one active film and one passive film. Only the active layer carries out thermal desorption or expansion during light exposure,[12,26,28,29] and the passive layer is inert to the thermal variation. Such a design limits the functionality of the bilayer structure, leading to the difficulty in the improvement of bending efficiency. Moreover, these actuators which own high amplitude (e.g., bilayer film actuated by thermal expansion), commonly require long response time. Similarly, most quick-reacting carbon actuators that are based on thermal desorption mechanism, can only bend in small angles limited by the water loss amount. Thus, continued efforts remain highly desired to integrate the high bending amplitude and speed into a single actuator. What is more, actuating strength and robustness should also be further enhanced for better robotic applications.

Herein, we propose a dual-active GO–PDA–gold nanoparticles (Au NPs)/PDMS bilayer film to realize high efficiency reversible light-driven actuation. In our design, we replace the conventional passive layer by one Au NPs enhanced thermal-responsive PDMS layer. We integrate two bending mechanisms with two thermal responsive layers: GO–PDA and PDMS, which can implement thermal desorption and expansion separately. The Au NPs are mixed to enhance the photothermal effect since noble metal nanoparticles can be used for obtaining remote and localized heating. The surface plasmon resonance of Au NPs strengthens the absorption and scattering of light due to coherent oscillations of metallic free electrons.[30,31] Assisted by Au NPs, the bilayer film exhibits better actuating performance, including higher bending amplitude and bending speed. Such a soft actuator can act as artificial arm as well as manipulator with high actuating strength. Furthermore, various locomotion modes, including linear, rolling, and steering motions are implemented with different structure designs with high locomotion flexibility.

Y. Yang. Dr. Y. Liu, Prof. Y. Shen
Department of Biomedical Engineering
City University of Hong Kong
999077 Hong Kong, China
E-mail: yajishen@cityu.edu.hk
Prof. Y. Shen
CityU Shen Zhen Research Institute
Shenzhen 518000, China

The ORCID identification number(s) for the author(s) of this article can be found under https://doi.org/10.1002/adfm.201910172.

DOI: 10.1002/adfm.201910172

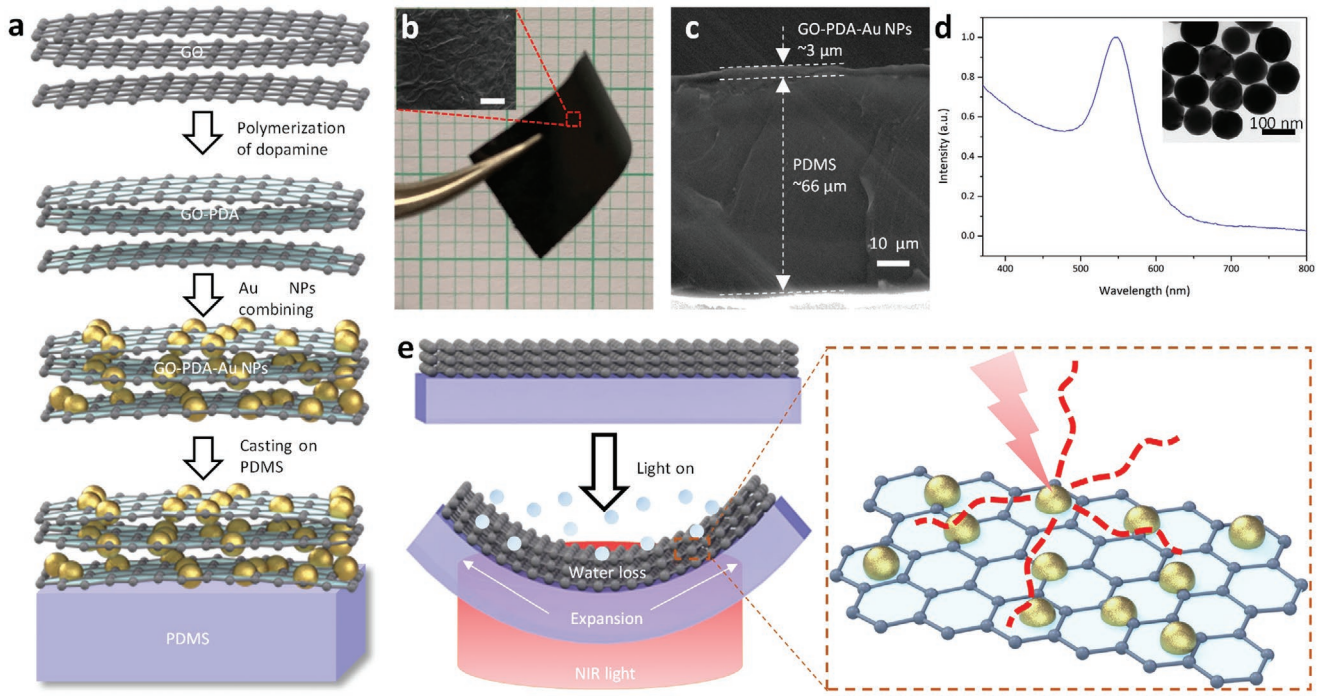

Figure 1. Plasmonic-assisted dual active bending mechanism and characterization of GO–PDA–Au NPs/PDMS composite film. a) Fabrication of bilayer film. b) Digital and SEM images of the composite film. c) Thickness of GO–PDA/Au NPs and PDMS layer is about 3 and 66 μm separately. d) Absorption spectrum and SEM image of Au NPs. e) Bending mechanism of the dual active bilayer structure, which integrates thermal expansion and desorption during light exposure. The photothermal effect is enhanced by the Au NPs.

2. Results and Discussion

The dual active bilayer GO–PDA–Au NPs/PDMS composite film is prepared through simple fabrication, as illustrated in **Figure 1**a and Figure S1 (Supporting Information). The thickness of GO–PDA–Au NPs layer and PDMS layer is ≈3 and 66 μm, respectively (Figure 1b,c). To enhance the photothermal effect of the composite film, Au NPs colloid is mixed in GO–PDA. The surface of Au NPs can heat quickly only within a few picoseconds of illumination. As the excitation dissipates via phonons, the surrounding GO–PDA, as well as PDMS, is heated. The size of Au NPs is roughly 85 nm, and the surface plasmon resonance of Au NPs is around 548 nm (Figure 1d). Figure S2 of the Supporting Information indicates that two main constituent elements (Au and C) are in the composite. The simulation of a single Au NP shows an enhancement of the electric field on the nanosphere surface with the 808 nm wavelength incident light (Figure S3, Supporting Information). Thus, a high light-to-heat conversion efficiency is expected. The plasmonic effect of Au NPs greatly facilitates the light-addressable bending of GO–PDA–Au NPs/PDMS composite films. The graphene material owns high thermal conductivity, which can convert light exposure into heat. By integrating the plasmonic effect of Au NPs, the thermal variation generates higher efficiency, which shortens the response time of actuation. The bending of the composite film is the integration of two mechanisms by the dual active bilayer structure (Figure 1e). One of which is the coefficient of thermal expansion (CTE) difference between the two layers. To be specific, PDMS owns high CTE (3×10^{-4} K^{-1}), which expands when the temperature increases.[32] However, the CTE of the GO–PDA–Au NPs layer is too low that almost no thermal expansion occurs. The another mechanism is thermal desorption. Increase in temperature induces water loss in the GO–PDA–Au NPs layer and no water variation in the PDMS layer. During NIR light exposure, two active layers are observed, that is, the GO–PDA–Au NPs layer shrinks while the PDMS layer expands, resulting in the bending of bilayer film. In addition, the plasma treatment of PDMS film during fabrication can increase the number of polar groups on its surface, which can enhance the surface wetting ability of PDMS and strengthen the bonding between two layers.

The GO–PDA–Au NPs/PDMS composite film exhibits advances in bending amplitude and speed over the conventional single layer-active bilayer film because of the dual active structure and plasmonic effect. To demonstrate this improvement quantitively, we set four control groups for comparison: rGO/PDMS, rGO–PDA/PDMS, GO/PDMS, and GO–PDA/PDMS bilayer film (for fabrication process, see the Supporting Information). To be specific, during NIR light exposure, thermal expansion occurs in the PDMS layer, water desorption in the rGO–PDA/PDMS, GO/PDMS, GO–PDA layer, and almost no shape deformation in the rGO layer. Thus, the rGO/PDMS group is based on a single active layer carrying out thermal expansion. Theoretically, the dual active rGO–PDA/PDMS, GO/PDMS, GO–PDA/PDMS group, which integrates two bending mechanisms, possesses a higher bending amplitude than rGO/PDMS group. As exhibited in **Figure 2**a, the composite films are cut into rectangles of 5 mm × 15 mm and exposed to NIR light with a laser power of 3 W cm^{-2} for 2 s. The bending angle of the GO–PDA/PDMS group (50°),

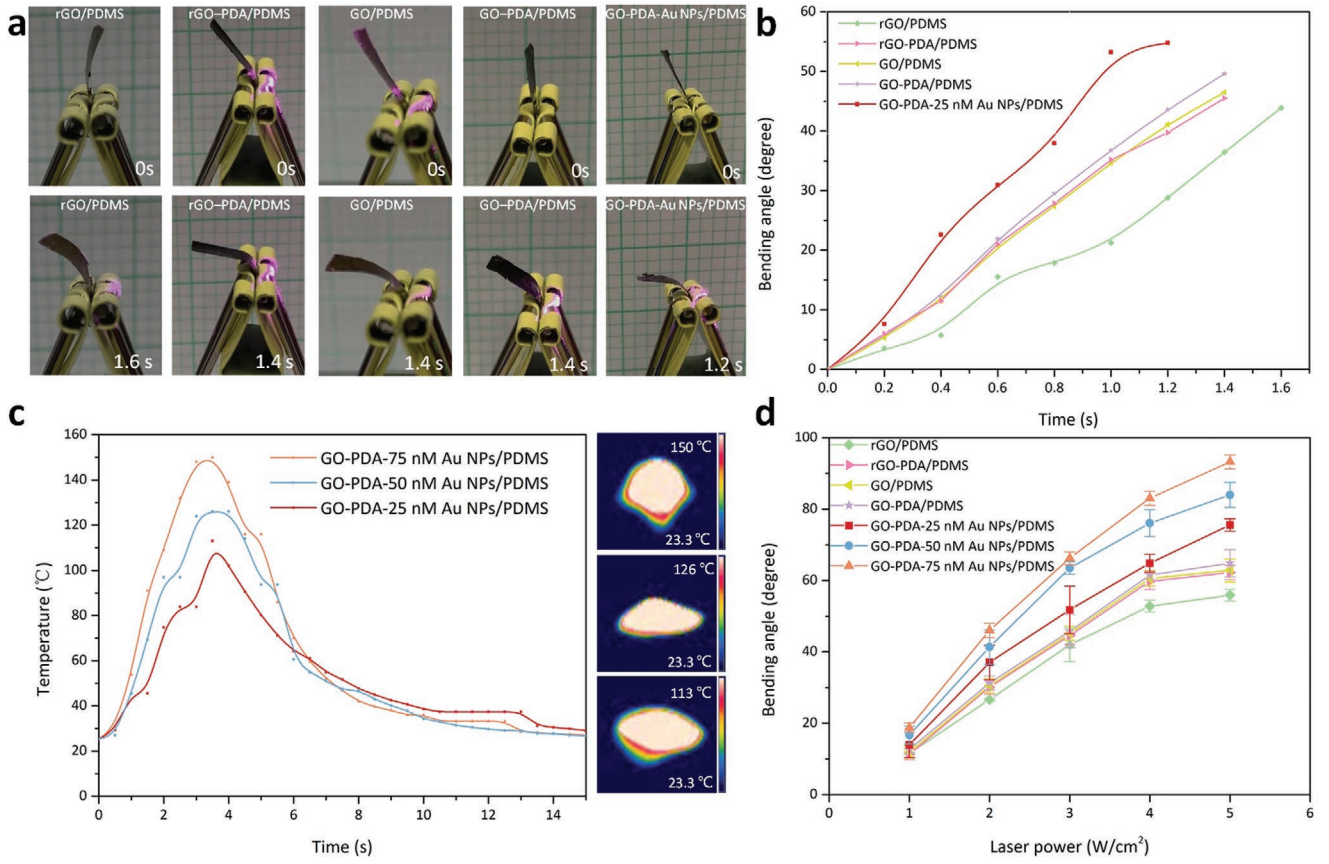

Figure 2. The GO–PDA–Au NPs/PDMS composite film demonstrates advances in bending amplitude and speed owning to the dual active structure and plasmonic effect. a) Digital images of the bending amplitude (rGO/PDMS, rGO–PDA/PDMS, GO/PDMS, GO–PDA/PDMS, GO–PDA–Au NPs/PDMS). b) Owing to the dual-active mechanism, the bending degree of rGO-PDA/PDMS, GO/PDMS, GO–PDA/PDMS composite film are higher than that of rGO/PDMS film. The GO–PDA–Au NPs/PDMS film bends in the highest degree benefited from the plasmonic effect of Au NPs. c) When NIR light exposure is applied, the concentration of Au NPs enhance the photothermal with large temperature variation. d) The GO–PDA–75 × 10^{-9} M Au NPs film bends in the highest degree under different laser power exposure.

rGO–PDA/PDMS group (47°), and GO/PDMS group (47°) are higher than that of the rGO/PDMS group (44°), verifying the superiority of the integrated bending mechanism (Figure 2b). Among these comparison groups, the GO–PDA/PDMS group shows better actuating performance due to the integrated water absorption/desorption ability of GO and DA. Furthermore, the heat transformation rate can be enhanced with the help of the plasmonic effect by Au NPs. As a result, the GO–PDA–Au NPs (25 × 10^{-9} M Au NPs) group owns the highest bending angle (55°) and the shortest response time, which is 1.2 s compared with those of rGO/PDMS, rGO–PDA/PDMS, GO/PDMS, and GO–PDA/PDMS groups, which are 1.4, 1.6, 1.6, and 1.6 s, respectively (Movie S1, Supporting Information). The bending angle of GO–PDA–Au NPs/PDMS bilayer film over 100 actuation cycles is shown in Figure S4 of the Supporting Information (laser power: 3 W cm^{-2}), demonstrating stable bending-recovery performance and good reversibility. For the same group of composite film, the bending angle is associated with the laser power applied. As exhibited in Figure S5 of the Supporting Information, with high laser power, the bending angle increases and the response time decreases. High laser power induces high temperature transfer and large shape change, including expansion and shrinkage of the active layers. Consequently, the interfacial force is enhanced. For the bilayer structure, the thickness of separate layer is also influential to the bending performance. With the same thickness of one layer, the bending amplitude of the composite film increases along with the thickness of another layer (Figure S6, Supporting Information).

To further demonstrate the function of Au NPs, we adjust the concentration of Au NPs colloidal solution into three groups containing 25, 50, and 75 × 10^{-9} M Au NPs. Figure 2c shows the thermal variation of the GO–PDA–Au NPs bilayer film with different Au NPs concentration during NIR light exposure. As exhibited, the temperature of GO–PDA–75 × 10^{-9} M Au NPs/PDMS group changes more quickly until nearly 150 °C (GO–PDA–25 × 10^{-9} M Au NPs/PDMS group: 113 °C; GO–PDA–50 × 10^{-9} M Au NPs/PDMS group: 126 °C), which exhibits the photothermal enhancement of Au NPs. Owning to the large temperature variation, the composite film with high Au NPs concentration bends with high bending amplitude and speed demonstrating the film's validity (Figure 2d). Compared with that of the rGO/PDMS group, the bending angle of GO–PDA–75 × 10^{-9} M Au NPs can be enhanced up to 173% and the response time is shortened by ≈50%. Thus, the bending speed

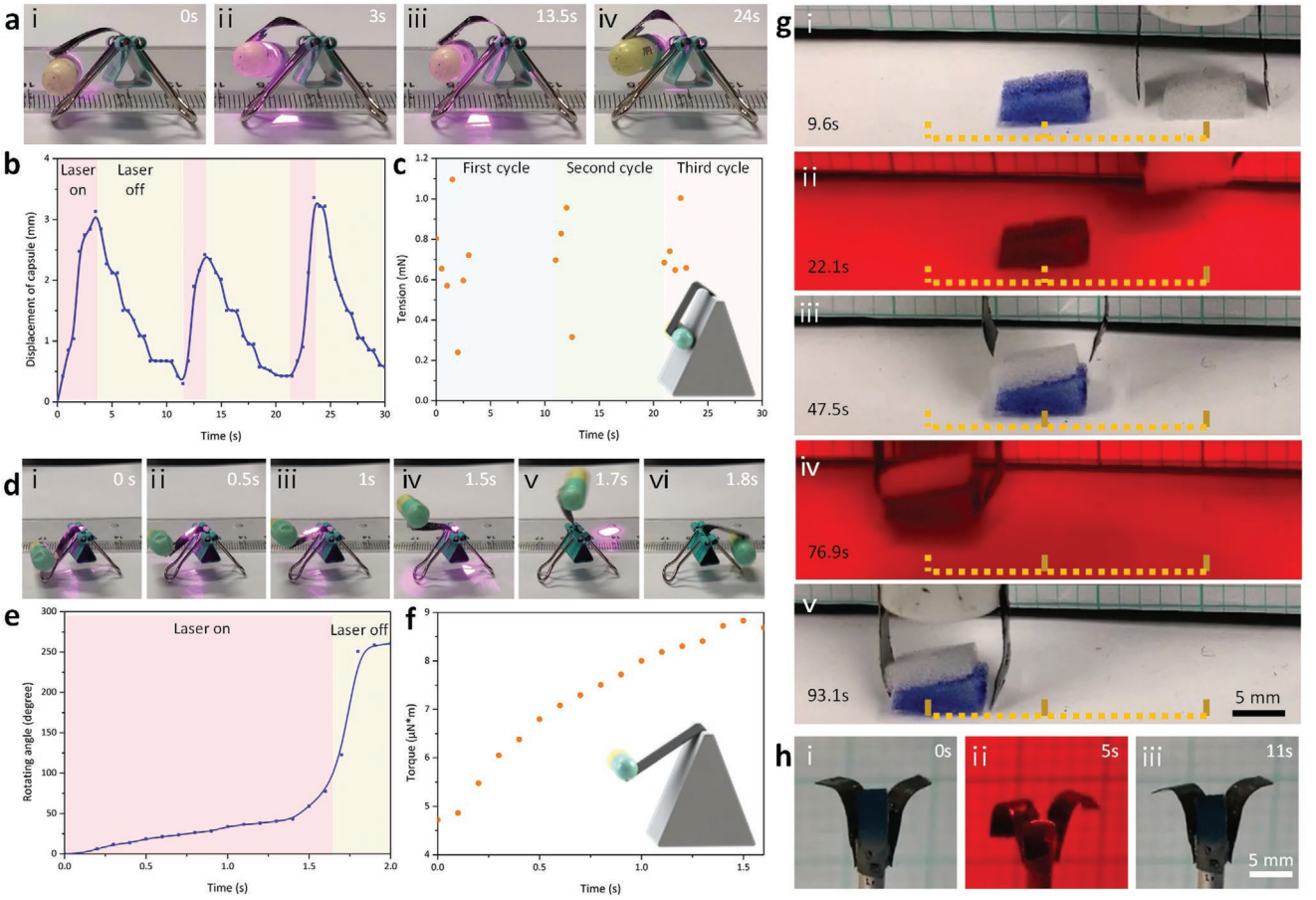

Figure 3. The GO–PDA–Au NPs/PDMS bilayer film exhibits sufficient actuating strength as artificial muscle. a) Digital images of the pulling motion implemented by bilayer film. b) Displacement of cargo during pulling motion. c) Corresponding tension force provided by composite film. d) Digital images of lifting motion implemented by bilayer film. e) Bending angle of the composite film during lifting motion. f) Corresponding torque provided by composite film. g) The bilayer film composed of artificial gripper can carry out picking and dropping tasks. h) The bilayer can take the place of petals mimicking the blooming of bioinspired artificial flower.

is improved 3.5 times. High actuating efficiency is observed compared with reported bilayer films such as GO–PDA/rGO actuator (bends to about 60° within 2 s)[26] and elastin-like polypeptides–rGO (bends to 75° within 5 s).[23]

Such advances provide the GO–PDA–Au NPs/PDMS bilayer film sufficient actuating strength, which allows it to be as an effective manipulator in robotic systems carrying out pulling, lifting, and grasping functions. Such a soft and flexible manipulator can avoid clamping force and enable the handling of objects with different shapes. To demonstrate, 88 mg cargo is stick to the composite film (**Figure 3**a). During the pulling motion, the bilayer is placed with PDMS upward, and the cargo is stick to the GO–PDA–Au NPs side. By applying light exposure, the bilayer bends downward, providing a pulling force to the cargo. The cargo is pulled up accordingly due to the contraction of the robot hand. After withdrawing the light exposure, the bilayer unbends, and the cargo returns to its original place (Movie S2, Supporting Information). The moving displacement of the cargo is shown in Figure 3b. The tension force of the actuator during 3 cycles is calibrated (Figure 3c), which could arrive at 1.1 mN during pulling process. To realize the lifting process, the bilayer film is inverted with the GO–PDA–Au NPs layer above. When applying light exposure, the bilayer film bends upward, lifting the cargo (Figure 3d; Movie S2, Supporting Information). During lifting process, the cargo rotates in the clockwise direction (Figure 3e). According to the rotation angle, the torque during lifting can be calculated up to 8.8 μN m (Figure 3f). The corresponding intensity of lifting force is up to 1.95 Pa, exhibiting excellent mechanical performance.

Furthermore, such an artificial muscle can act as a wireless soft manipulator to avoid damage to the cargo produced by clamping force. The soft manipulator is shown in Figure 3g, and it is composed of two bilayer films. With light exposure, the bilayer films bend inward and grip the cargo. To drop the cargo, light is removed to disable the bending, and clamping force disappears (Movie S3, Supporting Information). The light-actuated soft gripper can process several cargos, exhibiting high controllability and stability. This soft gripper possesses advantages such as short response time, high mechanical strength, and remote controllability, which can be applied in diverse robotic systems. The composite film can also act as an artificial muscle even for biomimetic systems. We take flower as an example. During the growth of flower, petals bloom from bud state to enable pollination. Inspired by this process, a 3D artificial flower is fabricated

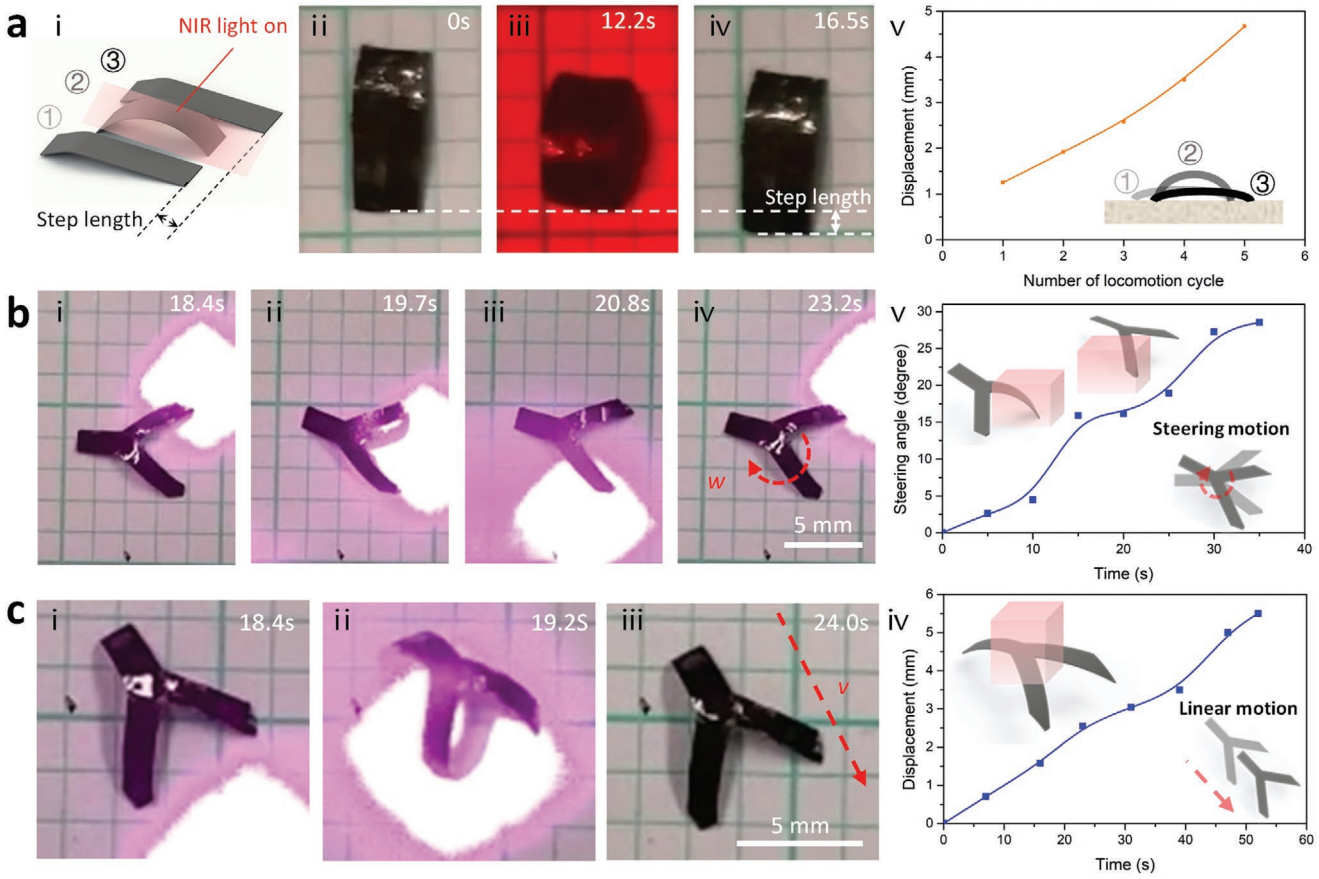

Figure 4. Soft robots are developed by different shape designs of the bilayer film exhibiting flexible locomotion ability. a) Shaped as a rectangle, the robot can effectively implement forward motion. The step length during one locomotion cycle is up to 1/6 of the robot body's length. b) The triple-legged robot can carry out steering motion when the NIR light spot is focused on two heads in sequence. c) The triple-legged robot can also move straight when the light spot focuses on the central robot body.

with three pieces of bilayer films acting as artificial petals. When actuated by NIR light, the three petals bend outward, mimicking the blooming process (Figure 3h). Without an external stimulus, the petals return to their original state, and the flower return to the bud state (Movie S4, Supporting Information). Such an artificial muscle can be applied in robotic manipulator tasks and biological systems, demonstrating high multifunctionality.

To explore other potential applications of the GO–PDA–Au NPs/PDMS film in robotic systems, soft robots capable of flexible locomotion are designed, which are inspired by reptiles. The forward linear motion can be simply implemented by the contraction and extension of the robot body. As shown in **Figure 4**a, the composite film is cut into a rectangle shape (7 mm × 4 mm) with slight unsymmetrical curvature. During one locomotion cycle, light-actuated bending induces the contraction of the robot body. Owing to the friction force difference between two ends, the robot body's barycenter moves forward. After removing light exposure, the robot body unbends and stretches forward (Figure S7 and Movie S5, Supporting Information). The step length for a separate cycle differs due to the bending angle error that can reach 1.25 mm, which is more than 1/6 of the robot body's length. The average walking speed during five locomotion cycles is ≈0.07 mm s^{-1}. As for designing the robot with irregular quadrangle shape like Figure S8a of the Supporting Information, different motions can be implemented according to varying laser exposure times in the rough surface. In this case, the light-actuated arching of the robot body leads to the point of contact between the robot and the ground. With short light exposure, the robot exhibits effective forward locomotion. As illustrated in Figure S8b, the step length during one locomotion cycle can achieve 1/2 of the robot body's length. Another motion—rolling motion—takes place with long-time NIR light exposure. When the light exposure time is adequately long, the unstable contact between the robot and the ground results in the rotation of the whole robot body so that the robot turns over (Figure S9, Supporting Information).

In addition to linear motion, the GO–PDA–Au NPs/PDMS film can enable steering motion by designing a multilegged robot structure, which offers opportunities for trajectory planning in practical applications. Here, we take the triple-legged structure for a simple demonstration. As exhibited in Figure 4b, the robot is fabricated with two symmetrical heads and a tail. By applying the light spot on two heads in sequence, the robot turns around accordingly. The locomotion mechanism is based on the different edge shapes of the two heads (Figure S10, Supporting Information). The average rotational

speed is roughly 0.82° s^{-1}. The linear motion can also be implemented by focusing the laser spot on the central robot body (Figure 4c; Figure S11, Supporting Information). Owing to the friction difference between the heads and the tail, the robot walks forward in the heads' direction with an average velocity of ≈0.11 mm s^{-1}. Thus, by changing the light exposure, the robot can implement different locomotion modes, exhibiting high flexibility (Movie S6, Supporting Information).

The design of GO–PDA–Au NPs/PDMS bilayer film integrates two thermal-responsive layers instead of the conventional one active layer/one passive layer structure. When exposed to light, water loss, and shape shrinkage in the GO–PDA–Au NPs layer and shape expansion in the PDMS layer occur simultaneously. Theoretically, quicker thermal desorption leads to shorter bending response time. However, the maximum shape deformation of the thermal desorption layer (GO–PDA layer) is determined by the water loss amount, which is usually limited and results in a small bending amplitude. The water loss amount is also highly related to several environmental elements, such as humidity. The bending amplitude of the thermal desorption mechanism is very low in dry environments compared with that in wet environments. By contrast, the environment variations have little effect on the thermal expansion layer (PDMS layer). Nonetheless, the extent of shape deformation is determined by the CTE of PDMS is fixed. Herein, we replace the passive layer by another thermal desorption layer, and the shrinkage volume of which amplifies the bending due to the interfacial force. With this dual active bilayer structure, high bending amplitude can be guaranteed in various environments with better robustness. As demonstrated in the experiment, the bending amplitude of GO–PDA/PDMS is higher than that of rGO/PDMS. Moreover, the bending speed is related to temperature variation, which can be further improved by enhancing the photothermal heating effect during light exposure. Light-sensitive Au NPs possessing high thermal conductivity is integrated, forming GO–PDA–Au NPs/PDMS bilayer film, which exhibits high bending speed and amplitude. Owing to the plasma treatment of PDMS layer, GO–PDA–Au NPs layer is combined with PDMS layer closely. Nevertheless, unstable bending performances including break apart or crack upon the NIR irradiation are noticed when the thickness of single layer is too high. The reason is that the bending resulted interfacial force exceeds the adhesive capacity of two layers. In case of thick composite film is in request, further chemical modification needs be implemented.

3. Conclusion

In conclusion, to enhance the bending performance of light-driven carbon-based bilayers, we develop a dual active GO–PDA–Au NPs/PDMS composite film. The bending of the fabricated bilayer film integrates thermal expansion and water desorption mechanisms. Moreover, Au NPs colloid is added to enhance the photothermal performance with the help of the plasmonic effect. According to the experiments, the GO–PDA–Au NPs/PDMS composite film possesses higher bending amplitude with short response time compared with rGO/PDMS, rGO–PDA/PDMS, GO/PDMS, and GO–PDA/PDMS films. Furthermore, the bending efficiency is enhanced with higher Au NPs concentration. Compared with the rGO/PDMS group, the bending angle increases up to 73%; the actuating speed, 3.5 times. The composite film is multifunctional with many potential applications. It can be applied as an artificial arm with high actuating strength (1.95 Pa). Such an artificial muscle can act as wireless soft gripper for robotic systems, avoiding clamping force while exhibiting good controllability and stability. The soft actuator can also be applied as artificial petals mimicking the blooming of a flower. Several locomotion modes, including the forward, rolling, and steering motion are demonstrated by the simple shape design of the composite film. Such soft actuator would offer new opportunities for biomimetic soft robotics as well as its future applications.

4. Experimental Section

Preparation of Au NPs: Au NPs (≈85 nm) were prepared by the modified Frens method.[33] Sodium citrate (2.2×10^{-3} M, 150 mL) solution was added in a 250 mL three-necked round-bottomed flask and mixed for 15 min under vigorous stirring. A magnetic heating platform was utilized to increase the reaction temperature. Upon boiling, 1 mL of $HAuCl_4$ (25×10^{-3} M) was injected. The color of the solution changed from yellow to bluish-gray and then to soft pink in 10 min. The resulting Au NPs (≈85 nm) can be obtained, and hence concentrated colloids were acquired by thrice-repeated centrifugation at 10 000 rpm with deionized water.

Preparation of GO–PDA–Au NPs Composite: At first, 7 mg DA was mixed with 15 mL 2 mg mL^{-1} GO solution and sonicated for 1 h. Then, the centrifugated Au NPs were added in the resulted solution for another hour of sonication. The PH value of mixed solution was adjusted to 8.5 using 1 mol mL^{-1} Tris solution and stirred for 12 h at 45 °C. Afterward, three groups of GO–PDA–Au NPs solution with different Au NPs concentration (25, 50, and 75×10^{-9} M) were obtained.

Fabrication of Bilayer Film: PDMS was prepared at a 10:1 weight ratio (base:curing agent) and under spinning coating on the glass substrate at the speed of 500 rpm for 15 s and 900 rpm for 30 s. Then, PDMS was cured at the temperature of 75 °C for 2 h and transferred to the dish ($r = 27$ mm). After plasma treatment on the PDMS surface, 5 mL of GO–PDA–Au NPs solution was poured into a dish and dried at 75 °C for 5 h. Such operation was repeated two more times, and the bilayer film was obtained by peeling off.

Characterization of Bilayer Film: The obtained film was characterized using field emission scanning electron microscopy (FEI Quanta 450 FESEM). To actuate the bending of the bilayer film, 808 nm fiber-coupled laser (MLL-III-808, Changchun New Industries Optoelectronics Technology Co., Ltd.) was used. The temperature variation during actuation was measured by an infrared camera (FLIR T600).

Supporting Information

Supporting Information is available from the Wiley Online Library or from the author.

Acknowledgements

Y.Y. and Y.L. contributed equally to this work. This work was support by the National Science Foundation of China (61922093, U1813211, and 61773326) and Hong Kong RGC General Research Fund (CityU 11214817).

Conflict of Interest

The authors declare no conflict of interest.

Keywords

carbon-based materials, dual active bilayers, plasmonic-enhanced effects, soft manipulators, soft robotics

Received: December 6, 2019
Revised: January 17, 2020
Published online:

[1] S. M. Mirvakili, I. W. Hunter, *Adv. Mater.* **2018**, *30*, 1704407.
[2] S. I. Rich, R. J. Wood, C. Majidi, *Nat. Electron.* **2018**, *1*, 102.
[3] L. Hines, K. Petersen, G. Z. Lum, M. Sitti, *Adv. Mater.* **2017**, *29*, 1603483.
[4] I. Must, F. Kaasik, I. Põldsalu, L. Mihkels, U. Johanson, A. Punning, A. Aabloo, *Adv. Eng. Mater.* **2015**, *17*, 84.
[5] T. Qiu, T.-C. Lee, A. G. Mark, K. I. Morozov, R. Münster, O. Mierka, S. Turek, A. M. Leshansky, P. Fischer, *Nat. Commun.* **2014**, *5*, 5119.
[6] Y. Yang, Z. Pei, Z. Li, Y. Wei, Y. Ji, *J. Am. Chem. Soc.* **2016**, *138*, 2118.
[7] A. Fargette, S. Neukirch, A. Antkowiak, *Phys. Rev. Lett.* **2014**, *112*, 137802.
[8] D. D. Han, Y. L. Zhang, J. N. Ma, Y. Q. Liu, B. Han, H. B. Sun, *Adv. Mater.* **2016**, *28*, 8328.
[9] Y. Dong, J. Wang, X. Guo, S. Yang, M. O. Ozen, P. Chen, X. Liu, W. Du, F. Xiao, U. Demirci, *Nat. Commun.* **2019**, *10*, 4087.
[10] H. K. Bisoyi, A. M. Urbas, Q. Li, *Adv. Opt. Mater.* **2018**, *6*, 1800458.
[11] O. M. Wani, H. Zeng, A. Priimagi, *Nat. Commun.* **2017**, *8*, 15546.
[12] G. Xu, M. Zhang, Q. Zhou, H. Chen, T. Gao, C. Li, G. Shi, *Nanoscale* **2017**, *9*, 17465.
[13] L. Li, J. Meng, C. Hou, Q. Zhang, Y. Li, H. Yu, H. Wang, *ACS Appl. Mater. Interfaces* **2018**, *10*, 15122.
[14] X. Lu, H. Zhang, G. Fei, B. Yu, X. Tong, H. Xia, Y. Zhao, *Adv. Mater.* **2018**, *30*, 1706597.
[15] Z. Cheng, T. Wang, X. Li, Y. Zhang, H. Yu, *ACS Appl. Mater. Interfaces* **2015**, *7*, 27494.
[16] H. K. Bisoyi, Q. Li, *Chem. Rev.* **2016**, *116*, 15089.
[17] B. Han, Y. L. Zhang, Q. D. Chen, H. B. Sun, *Adv. Funct. Mater.* **2018**, *28*, 1802235.
[18] Y.-Y. Gao, Y.-L. Zhang, B. Han, L. Zhu, B. Dong, H.-B. Sun, *ACS Appl. Mater. Interfaces* **2019**, *11*, 37130.
[19] D. D. Han, Y. L. Zhang, Y. Liu, Y. Q. Liu, H. B. Jiang, B. Han, X. Y. Fu, H. Ding, H. L. Xu, H. B. Sun, *Adv. Funct. Mater.* **2015**, *25*, 4548.
[20] Z. C. Jiang, Y. Y. Xiao, X. Tong, Y. Zhao, *Angew. Chem., Int. Ed.* **2019**, *58*, 5332.
[21] R. Yang, Y. Zhao, *Angew. Chem., Int. Ed.* **2017**, *56*, 14202.
[22] Y. Huang, J. Liang, Y. Chen, *J. Mater. Chem.* **2012**, *22*, 3671.
[23] E. Wang, M. S. Desai, S.-W. Lee, *Nano Lett.* **2013**, *13*, 2826.
[24] M. Yang, Z. Yuan, J. Liu, Z. Fang, L. Fang, D. Yu, Q. Li, *Adv. Opt. Mater.* **2019**, *7*, 1900069.
[25] L. Wang, H. K. Bisoyi, Z. Zheng, K. G. Gutierrez-Cuevas, G. Singh, S. Kumar, T. J. Bunning, Q. Li, *Mater. Today* **2017**, *20*, 230.
[26] J. Mu, C. Hou, H. Wang, Y. Li, Q. Zhang, M. Zhu, *Sci. Adv.* **2015**, *1*, e1500533.
[27] Y. Hu, J. Liu, L. Chang, L. Yang, A. Xu, K. Qi, P. Lu, G. Wu, W. Chen, Y. Wu, *Adv. Funct. Mater.* **2017**, *27*, 1704388.
[28] J. Li, R. Zhang, L. Mou, M. Jung de Andrade, X. Hu, K. Yu, J. Sun, T. Jia, Y. Dou, H. Chen, *Adv. Funct. Mater.* **2019**, *29*, 1808995.
[29] D. D. Han, Y. Q. Liu, J. N. Ma, J. W. Mao, Z. D. Chen, Y. L. Zhang, H. B. Sun, *Adv. Mater. Technol.* **2018**, *3*, 1800258.
[30] B. Han, Y. L. Zhang, L. Zhu, Y. Li, Z. C. Ma, Y. Q. Liu, X. L. Zhang, X. W. Cao, Q. D. Chen, C. W. Qiu, *Adv. Mater.* **2019**, *31*, 1806386.
[31] L. Wang, K. G. Gutierrez-Cuevas, H. K. Bisoyi, J. Xiang, G. Singh, R. Zola, S. Kumar, O. Lavrentovich, A. Urbas, Q. Li, *Chem. Commun.* **2015**, *51*, 15039.
[32] N. Bowden, W. T. Huck, K. E. Paul, G. M. Whitesides, *Appl. Phys. Lett.* **1999**, *75*, 2557.
[33] H. Xia, Y. Xiahou, P. Zhang, W. Ding, D. Wang, *Langmuir* **2016**, *32*, 5870.

